



Article

Solid-State Solar Energy Conversion from WO₃ Nano and Microstructures with Charge Transportation and Light-Scattering Characteristics

Juyoung Moon ^{1,†}, Woojun Shin ^{2,†}, Jung Tae Park ^{1,*} and Hongje Jang ^{2,*}

¹ Department of Chemical Engineering, Konkuk University, 120 Neungdong-ro, Gwangjin-gu, Seoul 05029, Korea

² Department of Chemistry, Kwangwoon University, 20 Gwangwoon-ro, Nowon-gu, Seoul 01897, Korea

* Correspondence: jtpark25@konkuk.ac.kr (J.T.P.); hjang@kw.ac.kr (H.J.); Tel.: +82-2-450-3538 (J.T.P.); +82-2-940-8320 (H.J.)

† These authors contributed equally to this work.

Received: 19 November 2019; Accepted: 12 December 2019; Published: 17 December 2019



Abstract: Solar energy conversion devices composed of highly crystalline gel polymers with disk-WO₃ nanostructure and plate-WO₃ microstructures (D-WO₃ and P-WO₃, respectively) exhibited higher power conversion efficiency than those with a gel electrolyte. In this study, D-WO₃ and P-WO₃ were prepared using a hydrothermal process and their structural and morphological features were investigated for application in solar energy conversion devices. The P-WO₃ solid-state electrolyte significantly enhanced the cell performance owing to its charge transportation and light-scattering characteristics. The P-WO₃ solid-state electrolyte showed a power conversion efficiency of 6.3%, which is higher than those of the gel (4.2%) and D-WO₃ solid-state (5.5%) electrolytes. The electro-chemical impedance spectroscopy (EIS), intensity-modulated voltage spectroscopy (IMVS), diffuse reflectance, and incident photon-to-current conversion efficiency (IPCE) analysis results showed that the P-WO₃ solid-state electrolyte showed improved charge transportation and light scattering, and hence enhanced the cell performance.

Keywords: solid-state electrolyte; tungsten oxide (WO₃); hydrothermal; charge transportation; solar energy conversion; light scattering; dye-sensitized solar cell

1. Introduction

As an alternative to fossil fuel-based devices, dye-sensitized solar cells (DSSCs) are considered as one of the promising next-generation energy devices. DSSCs can be prepared easily at a low cost [1]. Among the electrolytes used in DSSCs, liquid-state electrolytes have been studied extensively due to their high efficiency (~12%) [2–10]. However, liquid-state electrolytes exhibit instability because of leakage and evaporation, and hence find limited DSSC applications.

Owing to their thermal and long-term stability, solvent independence, and environmental safety, solid-state electrolytes have gained significant attention [11–16]. However, solid-state electrolytes with highly crystalline polymers show lower mobility and ionic conductivity than liquid-state electrolytes. To reduce the polymer crystallization, additional inorganic nanofillers can be introduced [17]. In addition, this improves the free volume, thereby improving the ion conductivity and mobility of the solid electrolyte [18].

Introduction of the light-scattering effect is a simple method to enhance the light-harvesting capacity of solid-state DSSCs (ssDSSCs). Various studies have been carried out on introducing light scattering or photonic crystal layers within the photoanode [19,20]. On the other hand, at the

photoanode, the nanomaterial-based light-scattering layer can undergo delayed charge transport due to the large number of grain boundaries, which limits the photovoltaic efficiency of ssDSSC. Hence, the use of nano or microstructured electrolytes is an efficient way to enhance the light-harvesting properties and to improve the short-circuit current density of ssDSSCs without inducing charge recombination.

In this study, we prepared a solid-state electrolyte consisting of disk-WO₃ (D-WO₃) nanostructures and plate-WO₃ (P-WO₃) microstructures for ssDSSCs. The D-WO₃ nanostructures and P-WO₃ microstructures were fabricated through the hydrothermal process. Manufactured D-WO₃ and P-WO₃ solid-state electrolytes were thoroughly characterized for material characteristics through scanning electron microscopy (SEM) and wide-angle X-ray scattering (WAXS), and for photovoltaic efficiencies by electrochemical impedance spectroscopy (EIS), incident photon-current conversion efficiency (IPCE) analysis, diffuse reflectance analysis, and intensity-modulated voltage spectroscopy (IMVS). As a control, a gel electrolyte was prepared without D-WO₃ nanostructures or P-WO₃ microstructures.

2. Experiment

2.1. Materials

Titanium isopropoxide, 4-tert-butylpyridine, poly (ethylene glycol) (PEG, $M_n = 10000$ g/mol), lithium iodide (LiI), chloroplatinic acid, sodium tungsten dihydrate (Na₂WO₄·2H₂O), 1-methyl-3-propylimidazolium iodide (MPII), I₂, ammonium oxalate ((NH₄)₂C₂O₄), and titanium diisopropoxide bis (acetylacetonate) 75 wt% (Ti(acac)₂OiPr₂) were purchased from Sigma Aldrich (St Louis, MO, USA). Commercial nano-TiO₂ paste (Ti-Nanoxide, D20) and ruthenium (Ru) sensitizer (N719) were purchased from Solaronix (Aubonne, Switzerland). Acetonitrile, ethyl alcohol, chloroform, and 2-propanol were purchased from J.T. Baker. Fluorine doped tin oxide (F-SnO₂)-conducting substrates (FTO glass, TEC7) were purchased from Pilkington (Sandouville, France). All the chemicals and solvents were as received.

2.2. Preparation of Disk-WO₃ (D-WO₃) Nanostructures

The D-WO₃ nanostructures were synthesized via a facile one-step hydrothermal process. In brief, 0.79 g of Na₂WO₄·2H₂O was dissolved in 45 mL of deionized water (>18 MΩm) at 25 °C. Then, 1 mL of 10 M HCl was added to the as-prepared solution under constant stirring followed by the introduction of 0.2 g of ammonium oxalate ((NH₄)₂C₂O₄). After 2 min of stirring, 30 mL of deionized water (>18 MΩm) was added to the reaction mixture with stirring for 30 min. The as-prepared D-WO₃ precursor solution was transferred and heated for 3 h at 140 °C in a 100 mL Teflon-lined stainless-steel autoclave reactor. The as obtained precipitate was then thermally treated at 400 °C for 2 h in air condition to obtain the D-WO₃ nanostructures.

2.3. Preparation of Plate-WO₃ (P-WO₃) Microstructures

The P-WO₃ microstructures were prepared using a facile one-step hydrothermal process. In brief, 0.231 g of Na₂WO₄·2H₂O was dissolved in 30 mL of deionized water (>18 MΩm) under stirring at 25 °C followed by the introduction of 10 mL of 3 M HCl, resulting in a precipitate. After stirring for 30 min, the resulting solution was transferred and heated for 3 h at 140 °C in a 100 mL Teflon-lined stainless-steel autoclave reactor. The precipitate was filtered, washed with distilled water and ethanol several times to reduce the ions possibly remaining in the products, and was dried in air. The as obtained precipitate was then thermally treated at 400 °C for 2 h in air condition to obtain the P-WO₃ microstructures.

2.4. Preparation of the D-WO₃ and P-WO₃ Solid-State Electrolytes

The D-WO₃ and P-WO₃ solid-state electrolytes were prepared using the solution-casting method. First, 1g of PEG was dissolved in 10 mL of acetonitrile. The concentrations of D-WO₃ and P-WO₃ were fixed at 1 wt% relative to PEG. The molar ratio of the ether group of PEG to two iodine salts (LiI, MPII) was fixed at 20, and the iodine (I₂) content was fixed at 10 wt% with respect to the iodine salt

(See Table S3). The solvent (acetonitrile) was completely evaporated by vacuum drying. As a control sample, a gel electrolyte was prepared using the same procedure without the D-WO₃ nanostructures and P-WO₃ microstructures.

2.5. Fabrication of Dye-Sensitized Solar Cells (DSSCs)

DSSCs with an active area of 0.4 cm² were prepared. A transparent FTO substrate was employed to prepare both the two electrodes (photoanodes and counter electrodes). For the photoanode, a Ti (IV) bis(ethyl acetoacetate) diisopropoxide solution was first spin-coated onto the FTO substrate and was then annealed stepwise to 450 °C and maintained at this temperature for 30 min. Then, a commercial nano-TiO₂ paste (Ti-Nanoxide, D20) was cast onto the FTO substrate using the doctor blade method followed by annealing at 450 °C for 30 min. The nanocrystalline TiO₂ photoanode (10 μm thickness) was sensitized overnight with 13 mg of a ruthenium dye (535-bisTBA, N719) dissolved in distilled ethanol (50 mL). Counter electrodes were prepared by spin coating a solution of 1 wt% H₂PtCl₆ in isopropanol onto the FTO substrate followed by annealing at 450 °C for 30 min. A dilute gel or solid-state electrolyte solution was cast onto a dye-adsorbed TiO₂ photoanode and was then evaporated for easy penetration through the nanopores of the TiO₂ photoanode. Then, a concentrated gel or solid-state electrolyte solution was cast onto the photoanode to minimize the time required for solvent evaporation and to prevent the formation of cavities between the photoanode and the counter electrode during the solvent evaporation. Then, both the photoanode and the counter electrodes were superposed together and were pressed between two glass plates in order to achieve slow solvent evaporation and to obtain a thin electrolyte layer. The cells were placed in a vacuum oven for the complete evaporation of the solvent for 24 h and were then sealed with an epoxy resin.

2.6. Characterization

The surface morphologies of the D-WO₃ nanostructures and P-WO₃ microstructures were observed using scanning electron microscopy (SEM) (Hitachi SU 8010, Hitachi High-Technologies Corporation, Abingdon, UK). Wide angle X-ray diffraction (WAXs) was carried out using a Rigaku 3-kW rotating-anode X-ray generator with Cu Kα radiation (λ = 1.5406 Å) operating at 30 kV and 100 mA. The two theta range was 15–65° and a scanning speed of 10°/min was used. Electrochemical impedance spectroscopy (EIS) measurements were carried out at the open-circuit voltage (*V*_{oc}) over the frequency range of 10^{−2}–10⁶ Hz with an amplitude of 10 mV. The incident photo to electron conversion efficiency (IPCE) spectra of the D-WO₃ nanostructures and P-WO₃ microstructures were obtained using a CE system (IVIUM Technologies, Eindhoven, Netherlands). The diffused reflectance spectra of the D-WO₃ nanostructures and P-WO₃ microstructures were recorded over the wavelength range of 400–800 nm using a ultraviolet (UV)-visible spectrophotometer (Hewlett-Packard, Hayward, CA, USA). Intensity-modulated voltage spectroscopy (IMVS) measurements were carried out on an electrochemical workstation equipped with a frequency response analyzer under a modulated red-light emitting diode (635 nm) driven by a source supply, which could provide both the direct current/alternating current (DC/AC) components of the illumination. Frequency was varied from 10^{−2} to 10⁴ Hz. Current density-voltage (*J*-*V*) measurements were carried out on a potentiostat (IVIUM Technologies, Eindhoven, Netherlands). The photovoltaic parameters of the nano and microstructures were determined using the following equations:

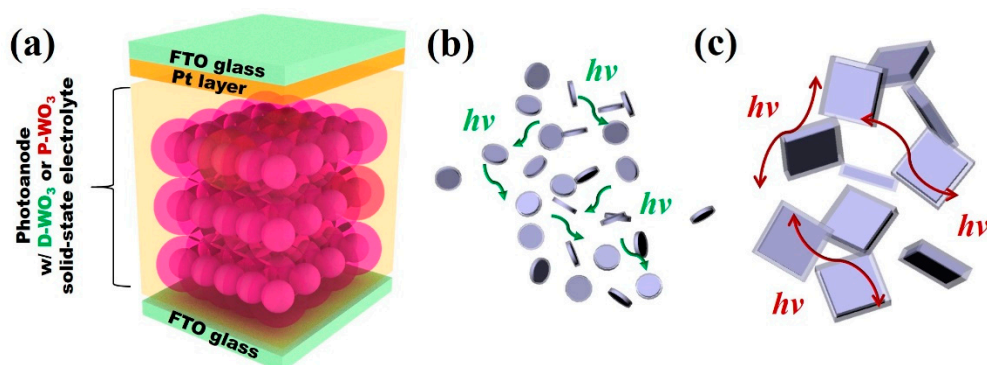
$$FF = V_{\max} J_{\max} / V_{oc} J_{sc} \quad (1)$$

$$\eta = V_{\max} J_{\max} / P_{in} 100 = V_{oc} J_{sc} FF / P_{in} 100 \quad (2)$$

where η is the solar power conversion efficiency (%), J_{sc} is the short circuit current density, V_{oc} is the open circuit voltage, P_{in} is the incident solar light power, and FF is the fill factor. J_{\max} and V_{\max} are the current density and voltage in the *J*-*V* curves of the structures at the maximum solar power output, respectively.

3. Results and Discussion

To improve the charge transportation and light scattering properties of the solid-state electrolyte, we employed P-WO₃ microstructures to create charge pathways and a light-scattering center, as shown in Scheme 1. The ssDSSC performance was improved by the P-WO₃ solid-state electrolyte, which facilitated the movement of the redox I⁻/I₃⁻ couple and enhanced the light-scattering characteristics of the ssDSSC. In order to survey the effect of the P-WO₃ solid-state electrolyte on the DSSC performance, gel and D-WO₃ solid-state electrolytes were also prepared.



Scheme 1. (a) Schematic of the dye-sensitized solar cells (DSSCs) fabricated in this study and the possible light scattering mechanisms of the (b) disk-WO₃ (D-WO₃) and (c) plate-WO₃ (P-WO₃) solid-state electrolytes.

Figure 1 exhibits the SEM image of the D-WO₃ nanostructures and P-WO₃ microstructures. The D-WO₃ nanostructures showed an average diameter of 300 nm. The P-WO₃ microstructures on the other hand, were approximately 5 μm in length. Gel electrolytes without nanofillers are transparent and show low light-scattering features. However, the P-WO₃ solid-state electrolyte showed rough layers owing to its irregular morphology. These layers showed light-scattering properties. The diffuse reflectance plots of DSSCs fabricated with gel electrolyte, D-WO₃ solid-state electrolytes, and P-WO₃ solid-state electrolytes were also measured by spectrophotometer (Figure S1). Hence, the P-WO₃ solid-state electrolyte showed better light harvesting than the gel and D-WO₃ solid-state electrolytes.

The WAXS results of the D-WO₃ nanostructures and P-WO₃ microstructures prepared using the hydrothermal process are shown in Figure 2. To acquire more quantitative information, the average crystalline WO₃ size was calculated using the following Scherrer equation:

$$D = k\lambda/\beta \cos\theta \quad (3)$$

where D is the average crystalline WO₃ size, k is the shape factor of the nanostructure, λ is the X-ray wavelength, β is the full width of the Bragg's diffraction peak at half its maximum intensity, and θ is half of the Bragg's diffraction angle of the center of the peak [13]. Both the D-WO₃ nanostructures and P-WO₃ microstructures exhibited WAXS peaks at $2\theta = 16.4, 25.6, 30.4, 33.3, 34.1, 35.0, 38.8, 48.5, 49.1, 49.6, 52.6, 56.1, \text{ and } 57.2$ corresponding to the (002), (111), (031), (040), (200), (002), (022), (240), (042), (222), (311), and (113) planes, respectively. These peaks could be indexed to the typical pattern of orthorhombic WO₃ (JCPDS No. 43-0679) [21]. These results confirm the successful preparation of highly crystalline orthorhombic D-WO₃ nanostructures and P-WO₃ microstructures from the WO₃ precursor using the hydrothermal process. All the WAXS peaks of the D-WO₃ nanostructures synthesized via the hydrothermal process were relatively wide, indicating that these nanostructures showed smaller crystallite size than the P-WO₃ microstructures. The average WO₃ crystallite size of the D-WO₃ nanostructures was estimated to be approximately 300 nm (using Equation (3)). This result is consistent with the nanostructure size obtained from the previous SEM image.

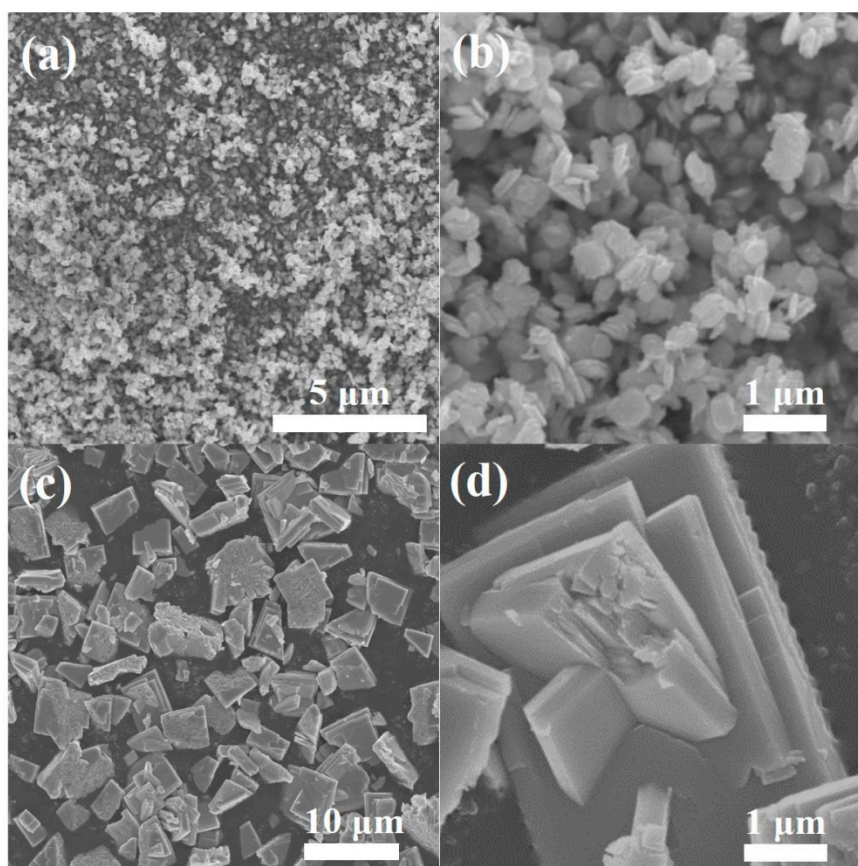


Figure 1. Scanning electron microscope (SEM) image of (a) D-WO₃, (b) magnified D-WO₃, (c) P-WO₃, and (d) magnified P-WO₃.

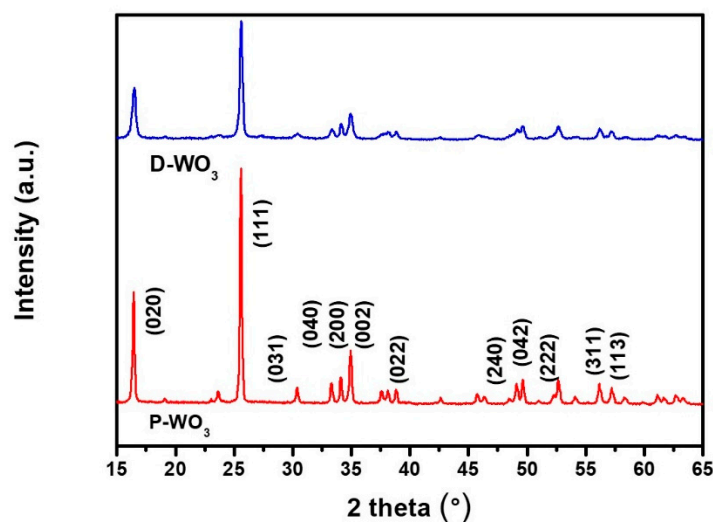


Figure 2. Wide-angle X-ray scattering (WAXS) results of D-WO₃ and P-WO₃.

EIS analysis was carried out at frequencies ranging from 10^{-2} Hz to 10^{-1} MHz with an AC amplitude of 0.02 V under 1 sun illumination. Figure 3a,b show the Nyquist plots and the equivalent circuit for the EIS spectra of the ssDSSCs employing the gel, D-WO₃ solid-state, and P-WO₃ solid-state electrolytes, respectively. The electro-kinetic characteristics, i.e., the interfacial resistance characteristics (R_s , R_1 , R_2 , and W_s) of the ssDSSCs are summarized in Table 1. R_s is the series interfacial resistance including the sheet resistance of the FTO substrate, R_1 is the charge transfer interfacial resistance of the counterelectrode, R_2 is the charge transfer interfacial resistance of the photoanode/sensitizer/electrolyte

interface, and W_s is the ionic diffusion within the electrolyte. CPE1 and CPE2 are the constant phase components of capacitance corresponding to R_1 and R_2 , respectively [22,23]. The total interfacial resistances of the ssDSSCs with the gel, D-WO₃ solid-state, and P-WO₃ solid-state electrolytes were 97.6, 60, and 63.9 Ω , respectively, as calculated using the EIS data fitted with the equivalent circuit. Because we used identical FTO substrates, photoanodes, and counter electrodes, the difference in the R_s and R_1 values was insignificant. Therefore, the difference in the total interfacial resistance, which was related with the R_2 value at the TiO₂ photoanode/sensitizer/electrolyte interface, of the three devices can be mainly associated to the solid-state electrolytes based on D-WO₃ and P-WO₃. The charge transfer interfacial resistances of the D-WO₃ ($R_2 = 42.9 \Omega$) and P-WO₃ ($R_2 = 43.4 \Omega$) solid-state electrolytes were lower than that of the gel electrolyte ($R_2 = 76.9 \Omega$). This can be attributed to the enhancement in the continuous free volumes related to ion-mobility resulting from the interaction between the WO₃ nano or microstructures and the highly crystalline polymer chain. In addition, the ionic diffusions within the P-WO₃ solid-state electrolyte (W_s) were slightly larger than those of the other systems. This result indicates that the viscosity of the P-WO₃ solid-state electrolyte was higher than those of the other electrolytes. Similar results have been reported previously [24]. To further understand the dynamics of charge transport, the recombination kinetics of the three types of cells were characterized by using dark EIS and IMVS (Figures S2 and S3).

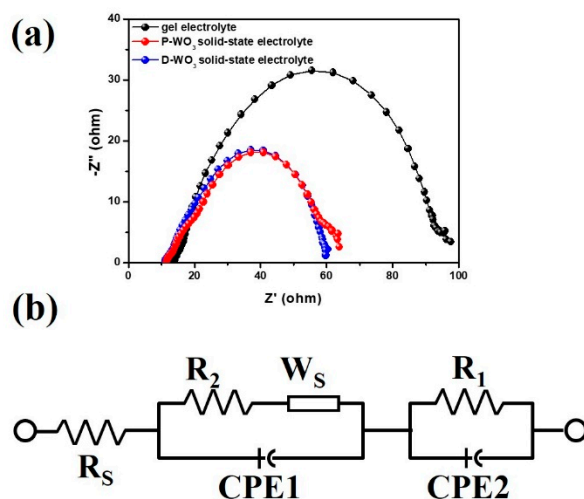


Figure 3. (a) Electro-chemical impedance spectroscopy (EIS) Nyquist plots of the DSSCs fabricated with the gel, D-WO₃ solid-state, and P-WO₃ solid-state electrolytes obtained under one sun illumination (AM 1.5, 100 mW cm⁻²) and (b) equivalent circuit of DSSCs.

Table 1. Photovoltaic and electrochemical properties of the DSSCs and ssDSSCs fabricated with the gel, D-WO₃ solid-state, and P-WO₃ solid-state electrolytes under 1 sun illumination (AM 1.5, 100 mW cm⁻²)^a.

Electrolyte	V_{oc} (V)	J_{sc}^b (mA/cm ²)	J_{sc}^c (mA/cm ²)	FF	η (%)	R_s	R_1	R_2	W_s
Gel	0.67 ± 0.2	11.1 ± 0.3	11.0	0.56 ± 0.02	4.2 ± 0.3	13.7	2.1	76.9	4.9
D-WO ₃ solid-state	0.74 ± 0.1	11.6 ± 0.3	11.8	0.64 ± 0.02	5.5 ± 0.2	11	2.5	42.9	3.6
P-WO ₃ solid-state	0.71 ± 0.1	14.6 ± 0.2	14.3	0.61 ± 0.02	6.3 ± 0.2	11.5	2.2	43.4	6.8

^a A typical dye-sensitized solar cell had an active area of 0.40/cm² and was masked using an aperture with similar area during the solar cell performance measurements. The thickness of the TiO₂ photoanode was about 7 μ m. ^b Determined from the J-V curves. ^c Determined from the incident photon-to-current conversion efficiency (IPCE) curves.

The IPCE analysis of the ssDSSCs provided quantitative information on their light-harvesting properties. Figure 4 exhibits the IPCE analysis of the ssDSSCs based on the gel, D-WO₃ solid-state, and P-WO₃ solid-state electrolytes. The P-WO₃ solid-state electrolyte-based DSSC exhibited a

maximum IPCE of 72% at a wavelength of about 540 nm while the gel electrolyte- and D-WO₃ solid-state electrolyte-based ssDSSCs showed the IPCEs of 45% and 52%, respectively. This indicates that the P-WO₃ solid-state electrolyte acted as an effective light-scattering center to enhance the scattering of the unabsorbed solar light back into the DSSC. Therefore, the P-WO₃ solid-state electrolyte improved the light-harvesting capability of the DSSC through efficient utilization of incident light.

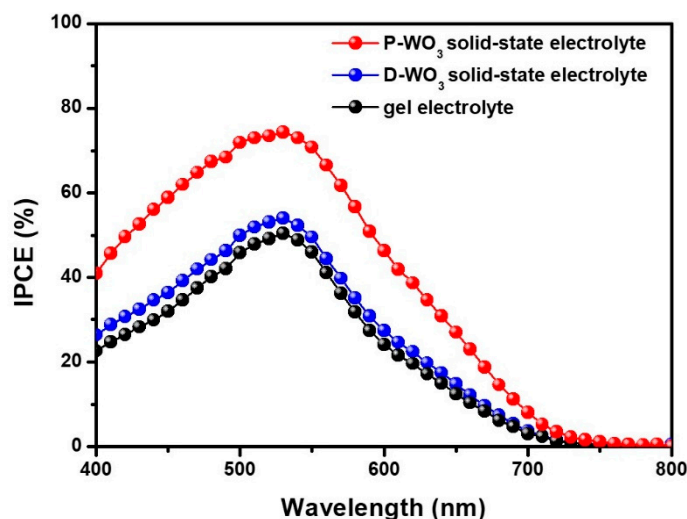


Figure 4. IPCE plots of the DSSCs fabricated with the gel, D-WO₃ solid-state, and P-WO₃ solid-state electrolytes.

Solid-state electrolytes with D-WO₃ nanostructures and P-WO₃ microstructures were prepared for fabricating DSSCs. The photovoltaic properties of the D-WO₃ and P-WO₃ solid-state electrolyte-based DSSCs are shown in Figure 5. Also, the performance of the liquid electrolyte was evaluated in DSSCs under on sun (AM 1.5) illumination (Figure 4, Table S2). The photovoltaic characteristics including the open-circuit voltage (V_{oc}), short-circuit current density (J_{sc}), fill factor (FF), and solar power conversion efficiency (η) of the DSSCs are listed in Table 1. The measurements were carried out under one sun illumination. As a control, a gel electrolyte was prepared using the same procedure without D-WO₃ nanostructures or P-WO₃ microstructures. The solid-state nanofiller ratio (1 wt%) was minimized to survey the effect of the morphology of the D-WO₃ nanostructures and P-WO₃ microstructures on the DSSC performance. The J_{sc} value of a device can be estimated by integrating its light harvesting, electron injection, and electron collection efficiencies using the following equation:

$$J_{sc} = q \eta_{lh} \eta_{inj} \cdot \eta_{col} I_0 \quad (4)$$

where q is the elementary charge, η_{lh} is the light harvesting efficiency, η_{inj} is the electron injection efficiency, η_{col} is the electron collection efficiency, and I_0 is the solar light flux [25,26]. The solar power conversion efficiencies of the ssDSSCs prepared with the D-WO₃ nanostructure- and P-WO₃ microstructure-based solid-state electrolytes were found to be 5.5 and 6.3%, at 100 mW/cm², which is one of the highest values for ssDSSCs (Table S1). These values are approximately 1.3- and 1.5-fold higher than that of the gel electrolyte-based DSSC, respectively. This result demonstrates the importance of incorporating inorganic WO₃ nanofillers in solid-state electrolytes. This enhancement in the DSSC performance with the incorporation the WO₃ nanofillers can be attributed to their high J_{sc} and FF values. According to Equation (4), light-harvesting characteristics were responsible for the high J_{sc} value of the ssDSSC based on the P-WO₃ solid-state electrolyte. Owing to the light-harvesting characteristics of P-WO₃, the light utilization efficiency of the ssDSSC improved along with an improve in the J_{sc} value. These results are consistent with the IPCE results shown in Figure 4. In addition, the D-WO₃ nanostructures and P-WO₃ microstructures acted as nanofillers and decreased the crystallinity

of the polymer electrolyte matrix, thus enhancing the continuous free volumes, charge-carrier mobility, and FF values of the ssDSSCs.

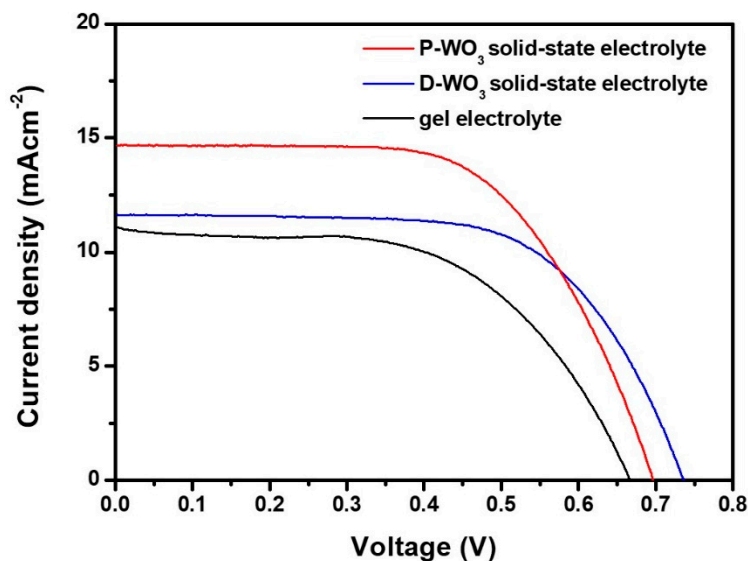


Figure 5. Current density-voltage (J - V) curves of the DSSCs fabricated with the gel, D-WO₃ solid-state, and P-WO₃ solid-state electrolytes obtained under one sun illumination (AM 1.5, 100 mW cm⁻²).

4. Conclusions

The solar power conversion efficiency of the P-WO₃ solid-state electrolyte-based ssDSSC was higher than those of the gel electrolyte- and D-WO₃ solid-state electrolyte-based DSSCs. The ssDSSC fabricated with the P-WO₃ solid-state electrolyte showed a solar power conversion efficiency of 6.3%, which is higher than those of the DSSCs with the gel (4.2%) and D-WO₃ solid-state (5.5%) electrolytes. P-WO₃ solid-state electrolytes offer enhanced charge transportation and light-scattering characteristics, can confine the incident light within the electrolyte/electrode, and limit the interfacial resistance, thereby increasing the cell performance. The results exhibited that the introduction of nano or microstructures within the non-electrode elements of DSSCs such as electrolytes can enhance the light-harvesting characteristic of the cells avoiding charge recombination, and hence increase their solar-energy conversion performance.

Supplementary Materials: The following are available online at <http://www.mdpi.com/2079-4991/9/12/1797/s1>, Figure S1: Diffuse reflectance plots of DSSCs fabricated with gel electrolyte, D-WO₃ solid-state electrolytes, and P-WO₃ solid-state electrolytes, Figure S2: EIS curves of DSSCs fabricated with gel electrolyte, D-WO₃ solid-state electrolytes, and P-WO₃ solid-state electrolytes measured at -0.65 V bias voltage in dark condition (100 kHz~10 mHz), Figure S3: IMVS of DSSCs fabricated with gel electrolyte, D-WO₃ solid-state electrolytes, and P-WO₃ solid-state electrolytes, Figure S4: J - V curves DSSCs fabricated with liquid electrolyte and P-WO₃ solid-state electrolytes that were obtained under one sun illumination (AM 1.5, 100 mW cm⁻²), Table S1: Comparison of photovoltaic parameters of DSSCs fabricated with polymer gel or solid-state electrolytes reported in the literature, Table S2: Photovoltaic parameters of DSSCs fabricated with liquid electrolyte and P-WO₃ solid-state electrolytes that were obtained under one sun illumination (AM 1.5, 100 mW cm⁻²), Table S3: DSSCs electrolyte formulations.

Author Contributions: Conceptualization, J.M.; formal analysis, W.S.; writing-review and editing, J.T.P. and H.J.

Funding: This work was supported by the National Research Foundation of Korea (NRF) grant funded by the Korea government (MSIP) (NRF-2019R1C1C1002305, NRF-2019R1C1C1010283) and the Technology Innovation Program (20004627) funded by the Ministry of Trade, Industry & Energy (MOTIE, Korea).

Conflicts of Interest: The authors declare no conflict of interest.

References

1. O'Regan, B.; Grätzel, M. A low-cost, high-efficiency solar cell based on dye sensitized colloidal TiO₂ films. *Nature* **1991**, *353*, 737. [[CrossRef](#)]

2. Sofyan, N.; Ridhova, A.; Yuwono, A.H.; Udhiarto, A.; Fergus, J.F. Synthesis of TiO₂ nanoparticles at low hydrothermal temperature and its performance for DSSC sensitized using natural dye extracted from *Melastoma malabathricum* L. seeds. *Int. J. Energy Res.* **2019**, *43*, 5959. [[CrossRef](#)]
3. Nazeeruddin, M.K.; Péchy, P.; Renouard, T.; Zakeeruddin, S.M.; Humphry-Baker, R.; Comte, P.; Liska, P.; Cevey, L.; Costa, E.; Shklover, V.; et al. Engineering of Efficient Panchromatic Sensitizers for Nanocrystalline TiO₂-Based Solar Cells. *J. Am. Chem. Soc.* **2001**, *123*, 1613–1624. [[CrossRef](#)] [[PubMed](#)]
4. Kakiage, K.; Aoyama, Y.; Yano, T.; Oya, K.; Fujisawa, J.; Hanaya, M. Highly-efficient dye-sensitized solar cells with collaborative sensitization by silyl-anchor and carboxy-anchor dyes. *Chem. Commun.* **2015**, *51*, 15894–15897. [[CrossRef](#)]
5. Shih, C.-M.; Wu, Y.-L.; Wang, Y.-C.; Kumar, S.R.; Tung, Y.-L.; Yang, C.-C.; Lue, S.J. Ionic transport and interfacial interaction of iodide/iodine redox mechanism in agarose electrolyte containing colloidal titanium dioxide nanoparticles. *J. Photochem. Photobiol. A Chem.* **2018**, *356*, 565–572. [[CrossRef](#)]
6. Yum, J.-H.; Baranoff, E.; Kessler, F.; Moehl, T.; Ahmad, S.; Bessho, T.; Marchioro, A.; Ghadiri, E.; Moser, J.-E.; Yi, C.; et al. A cobalt complex redox shuttle for dye-sensitized solar cells with high open-circuit potentials. *Nat. Commun.* **2012**, *3*, 631. [[CrossRef](#)]
7. Wang, D.; Zhang, Y.; Su, M.; Xu, T.; Yang, H.; Bi, S.; Zhang, X.; Fang, Y.; Zhao, J. Design of Morphology-Controllable ZnO Nanorods/Nanoparticles Composite for Enhanced Performance of Dye-Sensitized Solar Cells. *Nanomaterials* **2019**, *9*, 931. [[CrossRef](#)]
8. Zhang, Q.; Li, C. TiO₂ Coated ZnO Nanorods by Mist Chemical Vapor Deposition for Application as Photoanodes for Dye-Sensitized Solar Cells. *Nanomaterials* **2019**, *9*, 1339. [[CrossRef](#)]
9. Oprea, C.I.; Girtu, M.I. Structure and Electronic Properties of TiO₂ Nanoclusters and Dye–Nanocluster Systems Appropriate to Model Hybrid Photovoltaic or Photocatalytic Applications. *Nanomaterials* **2019**, *9*, 357. [[CrossRef](#)]
10. Jo, M.S.; Cho, J.S.; Wang, X.L.; Jin, E.M.; Jeong, S.M.; Kang, D.-W. Improving of the Photovoltaic Characteristics of Dye-Sensitized Solar Cells Using a Photoelectrode with Electrospun Porous TiO₂ Nanofibers. *Nanomaterials* **2019**, *9*, 95. [[CrossRef](#)]
11. Zhou, Y.; Xiang, W.; Chen, S.; Fang, S.; Zhou, X.; Zhang, J.; Lin, Y. Improvements of photocurrent by using modified SiO₂ in the poly(ether urethane)/poly(ethylene oxide) polymer electrolyte for all-solid-state dye-sensitized solar cells. *Chem. Commun.* **2009**, *26*, 3895–3897. [[CrossRef](#)] [[PubMed](#)]
12. Singh, P.K.; Bhattacharya, B.; Nagarale, R.K. Effect of nano-TiO₂ dispersion on PEO polymer electrolyte property. *J. Appl. Polym. Sci.* **2010**, *118*, 2976–2980. [[CrossRef](#)]
13. Park, J.T.; Lee, C.S.; Kim, J.H. High performance electrocatalyst consisting of CoS nanoparticles on an organized mesoporous SnO₂ film: Its use as a counter electrode for Pt-free, dye-sensitized solar cells. *Nanoscale* **2015**, *7*, 670–678. [[CrossRef](#)] [[PubMed](#)]
14. Chen, C.; Teng, H.; Lee, Y. In Situ Gelation of Electrolytes for Highly Efficient Gel-State Dye-Sensitized Solar Cells. *Adv. Mater.* **2011**, *23*, 4199–4204. [[CrossRef](#)] [[PubMed](#)]
15. Chen, C.-L.; Chang, T.-W.; Teng, H.; Wu, C.-G.; Chen, C.-Y.; Yang, Y.-M.; Lee, Y.-L. Highly efficient gel-state dye-sensitized solar cells prepared using poly(acrylonitrile-co-vinyl acetate) based polymer electrolytes. *Phys. Chem. Chem. Phys.* **2013**, *15*, 3640–3645. [[CrossRef](#)] [[PubMed](#)]
16. Kim, Y.J.; Kim, J.H.; Kang, M.; Lee, M.J.; Won, J.; Lee, J.C.; Kang, Y.S. Supramolecular Electrolytes for Use in Highly Efficient Dye-Sensitized Solar Cells. *Adv. Mater.* **2004**, *16*, 1753–1757. [[CrossRef](#)]
17. Iftikhar, H.; Sonai, G.G.; Hashmi, S.G.; Nogueira, A.F.; Lund, P.D. Progress on electrolytes development in dye-sensitized solar cells. *Materials* **2019**, *12*, 1998. [[CrossRef](#)]
18. Yoon, I.-N.; Song, H.-K.; Won, J.; Kang, Y.S. Shape dependence of SiO₂ nanomaterials in a quasi-solid electrolyte for application in dye-sensitized solar cells. *J. Phys. Chem. C* **2014**, *118*, 3918–3924. [[CrossRef](#)]
19. Shital, S.; Swami, S.K.; Barnes, P.; Dutta, V.J. Monte Carlo simulation for optimization of a simple and efficient bifacial DSSC with a scattering layer in the middle. *Sol. Energy* **2018**, *161*, 64–73. [[CrossRef](#)]
20. Liu, J.; Yao, M.; Shen, L. Third generation photovoltaic cells based on photonic crystals. *J. Mater. Chem. C* **2019**, *7*, 3121–3145. [[CrossRef](#)]
21. JCPDS, No. 43-0679. Available online: <http://www.icdd.com/> (accessed on 19 November 2019).
22. Li, X.; Pan, K.; Qu, Y.; Wang, G. One-dimension carbon self-doping g-C₃N₄ nanotubes: Synthesis and application in dye-sensitized solar cells. *Nano Res.* **2018**, *11*, 1322–1330. [[CrossRef](#)]

23. Park, J.T.; Chi, W.S.; Jeon, H.; Kim, J.H. Improved electron transfer and plasmonic effect in dye-sensitized solar cells with bi-functional Nb-doped TiO₂/Ag ternary nanostructures. *Nanoscale* **2014**, *6*, 2718–2729. [[CrossRef](#)] [[PubMed](#)]
24. Chi, W.S.; Roh, D.K.; Kim, S.J.; Heo, S.Y.; Kim, J.H. Hybrid electrolytes prepared from ionic liquid-grafted alumina for high-efficiency quasi-solid-state dye-sensitized solar cells. *Nanoscale* **2013**, *5*, 5341–5348. [[CrossRef](#)] [[PubMed](#)]
25. Guo, M.; Xie, K.; Lin, J.; Yong, Z.; Yip, C.T.; Zhou, L.; Wang, Y.; Huang, H. Design and coupling of multifunctional TiO₂ nanotube photonic crystal to nanocrystalline titania layer as semi-transparent photoanode for dye-sensitized solar cell. *Energy Environ. Sci.* **2012**, *5*, 9881–9888. [[CrossRef](#)]
26. Park, J.T.; Lee, C.S.; Kim, J.H. One-pot synthesis of hierarchical mesoporous SnO₂ spheres using a graft copolymer: Enhanced photovoltaic and photocatalytic performance. *RSC Adv.* **2014**, *4*, 31452–31461. [[CrossRef](#)]



© 2019 by the authors. Licensee MDPI, Basel, Switzerland. This article is an open access article distributed under the terms and conditions of the Creative Commons Attribution (CC BY) license (<http://creativecommons.org/licenses/by/4.0/>).